Improving osteoblasts cells proliferation via femtosecond laser surface modification of 3D-printed poly-ε-caprolactone scaffolds for bone tissue engineering applications

A. Daskalova, B. Ostrowska, A. Zhelyazkova, W. Święszkowski, A. Trifonov, H. Declercq, C. Nathala, K. Szlazak, M. Lojkowski, et al.

Applied Physics A
Materials Science & Processing

ISSN 0947-8396
Volume 124
Number 6

Appl. Phys. A (2018) 124:1-15
DOI 10.1007/s00339-018-1831-y

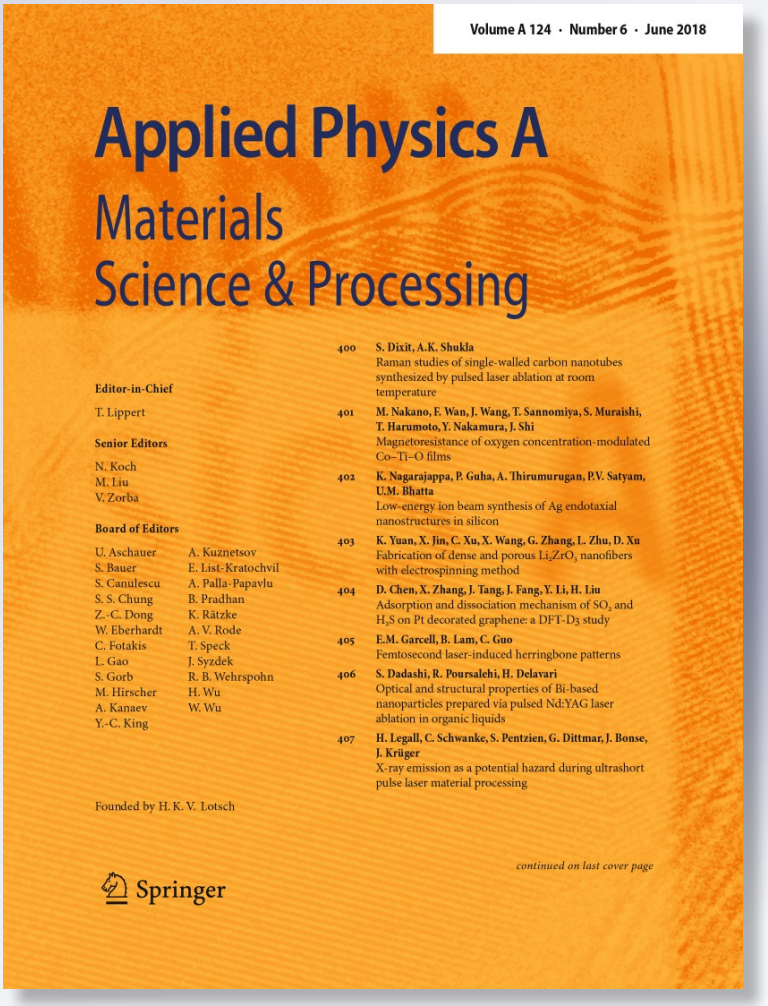

Springer

Applied Physics A (2018) 124:413
https://doi.org/10.1007/s00339-018-1831-y

Applied Physics A
Materials Science & Processing

Improving osteoblasts cells proliferation via femtosecond laser surface modification of 3D-printed poly-ε-caprolactone scaffolds for bone tissue engineering applications

A. Daskalova[1] · B. Ostrowska[2] · A. Zhelyazkova[1] · W. Święszkowski[2] · A. Trifonov[3] · H. Declercq[4] · C. Nathala[6] · K. Szlazak[2] · M. Lojkowski[2] · W. Husinsky[5] · I. Buchvarov[3]

Received: 16 February 2018 / Accepted: 30 April 2018 / Published online: 8 May 2018

Abstract
Synthetic polymer biomaterials incorporating cells are a promising technique for treatment of orthopedic injuries. To enhance the integration of biomaterials into the human body, additional functionalization of the scaffold surface should be carried out that would assist one in mimicking the natural cellular environment. In this study, we examined poly-ε-caprolactone (PCL) fiber matrices in view of optimizing the porous properties of the constructs. Altering the porosity of a PCL scaffold is expected to improve the material's biocompatibility, thus influencing its osteoconductivity and osteointegration. We produced 3D poly-ε-caprolactone (PCL) matrices by a fused deposition modeling method for bone and cartilage tissue engineering and performed femtosecond (fs) laser modification experiments to improve the surface properties of the PCL construct. Femtosecond laser processing is one of the useful tools for creating a vast diversity of surface patterns with reproducibility and precision. The processed surface of the PCL matrix was examined to follow the effect of the laser parameters, namely the laser pulse energy and repetition rate and the number (N) of applied pulses. The modified zones were characterized by scanning electron microscopy (SEM), confocal microscopy, X-ray computed tomography and contact angle measurements. The results obtained demonstrated changes in the morphology of the processed surface. A decrease in the water contact angle was also seen after fs laser processing of fiber meshes. Our work demonstrated that a precise control of material surface properties could be achieved by applying a different number of laser pulses at various laser fluence values. We concluded that the structural features of the matrix remain unaffected and can be successfully modified through laser postmodification. The cells tests indicated that the micro-modifications created induced MG63 and MC3T3 osteoblast cellular orientation. The analysis of the MG63 and MC3T3 osteoblast attachment suggested regulation of cells volume migration.

1 Introduction

Different natural polymers (collagen, gelatin, chitosan, etc.) and synthetic polymers [poly-l-lactide (PLLA), polydimethysiloxane (PDMS), polymethylmethacrylate (PMMA), poly lactide-*co*-glycotide (PLGA), poly-ε-caprolactone (PCL), etc.] have been investigated mainly for bone repair applications [1]. The engineered scaffolds have to be constructed in a 3D form with graded porosity sustainable to environmental conditions to guarantee stable cells adhesion, proliferation and differentiation. Synthetic polymers are widely used as substitute matrices since they can be fabricated easily in desired forms and are less expensive. PCL is a synthetic polyester, a widely used biomaterial for engineering scaffold matrices for bone graft substitutes [2]. It possesses properties that are essential for an artificial construct, such as structural and mechanical stability, a considerable

✉ A. Daskalova
a_daskalova@code.bg

[1] Institute of Electronics, Bulgarian Academy of Sciences, 72, Tsarigradsko Chaussee blvd., 1784 Sofia, Bulgaria

[2] Faculty of Materials Science and Engineering, Warsaw University of Technology, 141 Woloska Str., 02-507 Warsaw, Poland

[3] Physics Department, Sofia University "St. Kliment Ohridski", 5 J. Bourchier Blvd., 1164 Sofia, Bulgaria

[4] Department of Basic Medical Sciences, Ghent University, De Pintelaan 185 6B3, 9000 Ghent, Belgium

[5] Institute of General Physics, Vienna University of Technology, Wiedner Hauptstr. 8-10/134, 1040 Vienna, Austria

[6] High Q Lasers GmbH, Feldgut 9, 6830 Rankweil, Austria

degree of biocompatibility and biodegradability and slow bioresorption [3].

Although the PCL material demonstrates excellent mechanical characteristics, it suffers from some disadvantages related to its biological functionality which can lead to weak cell–implant interactions [4]. Insufficient cell adhesion and reduced bioactivity are the main problems which arise with the application of the PCL in tissue regeneration. Some of the methods to overcome this issue are related to reinforcement by various kinds of bioceramics incorporation to promote the material's physical and biological properties. The results revealed that interactions between the ionic products from the bioceramics and osteoblasts cells are thus stimulated [5, 6]. Hosseini et al. [7] have investigated the creation of hybrid scaffolds composed of various concentrations diopside nanopowder embedded in PCL electrospun nanofibers with improved tensile strength and elastic modulus. They have demonstrated that the supplement of diopside nanopowder significantly enhances the bioactivity and degradation rate of the scaffolds compared to pure PCL.

Other attempts to optimize the PCL scaffolds' properties have been performed to achieve improved osteoinduction by influencing the construct porosity, using polyethylene glycol, sucrose, fructose and Ca^{2+} alginate as pore-genic agents. PCL scaffolds with three-dimensional porous structures fabricated by phase separation technique were produced; however, the enlarged void volume obtained reduced the scaffolds' mechanical strength [8]. The studies of Yu et al. [9] have demonstrated the effect of various amounts of sodium chloride (NaCl) as pore-genic agents on the porosity of PCL–hydroxyapatite (HA) scaffolds. The correlation between the particles size and concentration was shown to lead to the formation of more PCL-HA pore interconnections at higher concentration and a larger particle size, which compromised the mechanical properties of the scaffold. The methods of improving the properties of a given surface and creating a bioactive surface typically involve chemical treatment. One approach is chemical immobilization, which is usually achieved by deposition of an initially immobilized layer that forms conglomerates with an appropriate protein that is supplemented subsequently [10, 11]. Thus, orientation of intact proteins is achieved. One significant difficulty of this approach is that polymer surfaces do not exhibit most of the functionality required to ensure a stable binding of the biological agent; as a consequence, a deficiency in its activity may arise.

An appropriate scaffold design is characterized by an excellent biocompatibility and a controllable degradation kinetics. In the literature, there exist various reports on techniques applied for additional treatment for improvement of surface characteristics of polymer fiber meshes and layers, as plasma treatment, ion-beam modification, chemical etching [12–14]. The plasma modification of biodegradable PCL nanofibers is an alternative method for improvement of their biocompatibility. Manakhov et al. [15] have shown that the deposition of amine and carboxyl-anhydride plasma coatings onto the PCL nanofibers sufficiently improved the cell adhesion and viability. However, the presence of residuals is the most significant problem facing these techniques due to the risks of toxicity and carcinogenicity it poses to cells.

The femtosecond laser enhanced surface modification is an attractive approach, since it is contactless and is usually completed in one step that does not require any additional chemicals or materials. It provides a possibility to treat the material surface with a high degree of precision in comparison to other techniques [16, 17].

However, to the best of our knowledge, no systematic studies have been published regarding the influence of laser-induced modification on the surface of fibers matrices in view of improving cell attachment. The microporosity has to be carefully considered when designing scaffold matrices, since it is an important condition for cell viability and tissue ingrowth. An interconnected pore structure will permit inwards diffusion of oxygen and nutrients and outwards diffusion of waste products from the scaffold [18]. Porosity is essential factor for facilitating cell dynamics into the scaffold volume. It has been demonstrated by Zeltinger et al [19] that the scaffold pore density and size influence to great extent cellular growth and adhesion. Previous studies of designing electrospun PCL nanofibers have been shown by Lim et al [20] to influence surface porosity by laser processing without affecting the fiber surface.

Our experimental findings report on novel implementation of femtosecond laser ablation method to alter the fiber surface and porosity of 3D-printed PCL matrices. 3D-printed scaffolds possess controllable features; despite this high level of design precision, the porosity and high specific surface area of the fiber meshes are limited for some applications in regenerative medicine. Vast of biological studies with 3D-printed PCL meshes show that cells adhere on the surface of the meshes. Introducing an additional porosity by creating craters without affecting the nature of the polymer fibers via laser processing to enhance bioactivity of the scaffold is being applied.

The laser-assisted techniques present a promising alternative to the chemical methods, as lasers could be used to alter the material surface properties by micropatterning, thus designing adhesive surfaces that would help to regulate the collective cell response. Fabrication of textured surfaces by laser-assisted methods can influence the proteins adhesion, thus creating a bioactive surface.

In the research presented, we examined the possibilities of femtosecond laser processing to modify the topography of PCL microfibers by enhancing the porosity of the PCL scaffold.

A number of studies have shown that different surface textures affect the cell response [21–23]. Various patterning geometries, as pillars, pits, gratings, tubular patterning, grooves [24–26] can alter the surface topography, thus tuning the cells' behavior. Moreover, surface texturing increases the surface area and improves the adsorption of proteins and the connection between the cells and the scaffold surface.

Femtosecond laser microprocessing has been proven to be an excellent method for production of a variety of patterning designs in many materials. The essential characteristics that make femtosecond laser-material interaction favorable compared to the nano- and picosecond processing regimes are the fast and localized energy deposition, the absence of collateral damage, the negligible heat-affected zones, and the practical absence of a liquid phase [27, 28]. The femtosecond ablation process can be precisely tuned by regulating the material removal in depth.

In the present work, we constructed woodpile matrices from PCL and post-modified the designed scaffold by femtosecond laser irradiation. The changes in the material's properties (morphology, porosity, wettability) after laser processing were studied by different techniques. The preliminary studies of the modification effect over the MG63 osteoblast-like and MC3T3 cell line viability and orientation demonstrated the effectiveness of the proposed approach. Cell cultivation tests demonstrated the excellent viability of the cells cultured on modified PCL fiber meshes. The adhesion and orientation were also monitored of the osteoblasts cells with respect to the laser-produced micro-modifications. This indicates that the scaffolds are able to provide a suitable environment and support the growth and proliferation of cells. These results clearly indicated that the laser-treated scaffold provided adequate, sufficient surface for cell adhesion, proliferation and could have the ability to make direct bond to living cells implanted in the body.

The main issues addressed in this study were precise post-modification of the 3D PCL structures while preserving the primary constructs form, evaluation of the processing limits in lateral and volumetric dimensions and determination of the processing productivity.

In our experiment, laser-assisted processing method was applied by focusing the beam on the surface of the PCL fiber mesh. In this regime of processing, ablation of the sample material occurred after several consecutive pulses impinging on the fiber's surface. Such conditions for surface treatment are attractive for enlargement of area of interaction between cells and scaffold material, leading to improvement of hydrophilic properties, which are a key factor for cell proliferation. Selective surface treatment enhances the surface wettability and porosity of PCL scaffold without influencing the scaffold integrity. One important property of this type of microstructuring is the ability to adjust the dimensions of the fabricated patterns by precisely controlling applied laser parameters. To perform in-depth structuring of the scaffold, future experiments are foreseen in order to alter the bulk properties of the PCL matrix by employing laser beam focusing on the bulk. Different micro-modifications were introduced on the PCL fibers surface using femtosecond laser pulses to control the scaffold porosity and optimize the cellular ingrowth.

2 Experimental methods

2.1 3D structure designs

Poly-ε-caprolactone material with a molecular weight (M_n) of 45 kDa, a melt index of 0.95 g/10 min at 95 °C (ISO1133), a melting temperature of 57 °C, and a glass-transition temperature of − 60 °C were purchased from Sigma-Aldrich. To synthesize the scaffolds, three-dimensional (5×5 mm^2 in width and 3 mm in height) woodpile constructs from poly-ε-caprolactone (PCL) were designed using Solid Works 3D CAD Design Software. The geometrical model of the scaffold was then exported to a Bioscaffolder machine (SYSENG, Germany) as an STL file. Then, the internal architecture of the tested platforms was designed with lay-down patterns 0/90/180 (Fig. 1a).

Briefly, PCL granules were placed in a stainless-steel reservoir and heated to $T = 70$ °C by a heated cartridge unit. After melting, an air pressure of 5 bar was applied to the reservoir to transfer the molten polymer to an endless extrusion screw jacket with spindle speed of 120 rpm. The material was then extruded through a 250-µm needle on a base plate with a deposition speed of 95 mm/min. The technical parameters of the layer-by-layer plotted fibrous

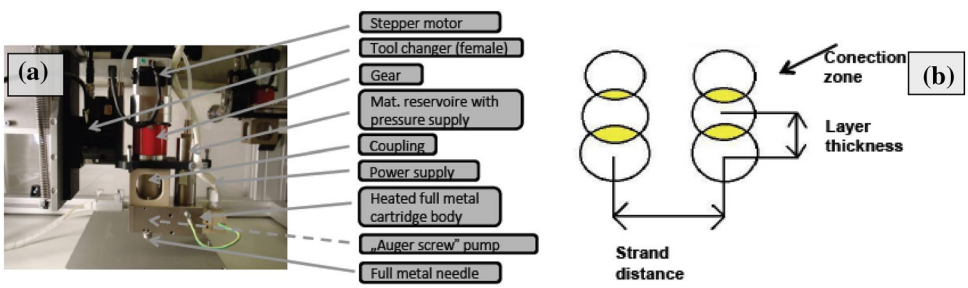

Fig. 1 Experimental configuration of Bioscaffolder machine (**a**); schematic diagram of fibers interconnection (**b**)

scaffolds were: spacing between fibers in the same layer of 140 µm, layer thickness of 160 mm; the configuration of the deposited fibers was varied by the layer deposition angle (90°) (Fig. 1b).

For the femtosecond laser modification experiments, we used two laser systems with different pulse durations to compare the processing outcome, namely a CPA multi-pass Ti:sapphire laser (Femtopower-Compact pro) emitting at a central wavelength of 800 nm with a temporal pulse width of $\tau = 30$ fs, a repetition rate of 1 kHz and a maximum energy of $E = 1$ mJ; and a Quantronix-Integra-C laser system delivering pulses of $\tau = 130$ fs at $\lambda = 800$ nm with a repetition rate ν varied—25 Hz, 50 Hz, and 1 kHz—by a delay generator. The number of applied laser pulses (N) was controlled by a computer-driven fast mechanical shutter and synchronized by the controlling software. The experiments were performed in air with the laser beam focused using a lens of focal length 20 cm at normal incidence. The sample was placed perpendicularly to the incident laser beam with the sample surfaces positioned close to the focal plane of a focusing lens on a high-precision XYZ translation stage (Fig. 2) and irradiated in a scanning mode with different fluences, number of pulses and repetition rates.

At this position, $1/e^2$ beam waist diameter of $2\omega_0 = 50$ µm was determined for focused laser beam. The focusing lens was placed on a translation stage with a micrometer screw for fine adjustment of the focus position on the specimen's working surface. All fluence values, F, mentioned in the article are peak fluences calculated by applying $F = 2 \times E/\pi \times \omega_0^2$, where E is the pulse energy and ω_0 is the beam radius. The laser fluence was estimated for each number of pulses N, using the method proposed by Liu [29]. This method is advantageous since it does not require a characterization of the laser beam. The laser beam had a Gaussian energy distribution.

The experimental setup was controlled by specially written LabView software. One of the advantages of this technique consists in the ability to tune the dimensions of the created patterns with high precision by controlling the laser parameters.

We estimated the material response to selected laser processing parameters [laser fluence (F), pulse repetition rate (ν), number of applied laser pulses (N)]. The contact angle measurements were performed using a goniometer. A drop of 1 µl distilled water was positioned on the surface of the processed material by a micro-syringe. The irradiated samples were examined using a scanning electron microscope (SEM) and confocal microscope. Cell culture experiments are performed by examining the cell orientation and migration on the femtosecond-laser-modified PCL constructs.

2.2 Scanning electron microscopy (SEM) and confocal microscopy surface analysis

The scaffolds' morphology was studied using scanning electron microscopy (SEM, SU8000 HITACHI), with the samples being coated beforehand by gold sputtering (Leica EM SCD 500). Figure 3 presents SEM images of the PCL matrices without laser processing. The samples prepared had a woodpile structure composed of 19 layers and 13 fibers. The average fiber diameter obtained was 209 µm and the average distance between the fibers was ~ 148 µm (Fig. 3).

The topography of the irradiated PCL scaffolds was examined using a µsurf explorer confocal microscope (Nanofocus). The apparatus provides high-resolution images of the surface and quantitative measurement of the surface roughness and the coating thickness. It gives further information about the size and the range of the surface undulations. The surface profiles were displayed as contour images.

2.3 X-ray computed tomography

The 3D structure and internal architecture were also investigated by micro-computed tomographical analysis (SkyScan 1172, Bruker). The X-ray tomography was employed to scan the whole sample scaffold in its initial state and after

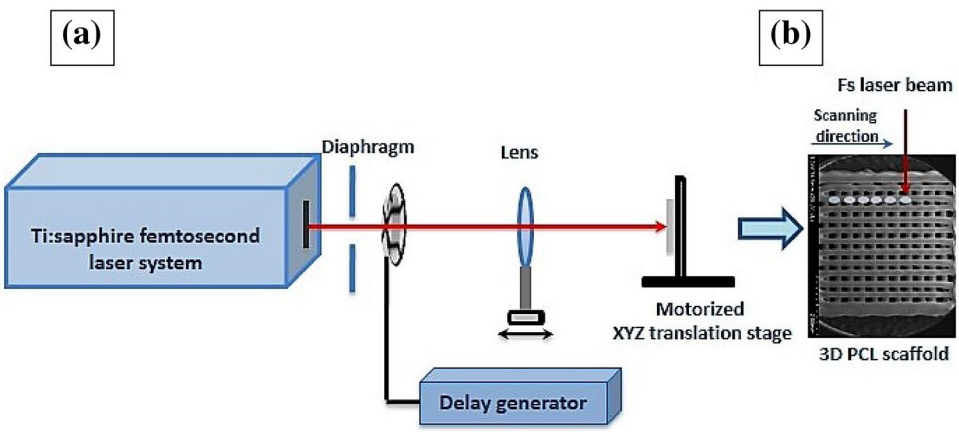

Fig. 2 Experimental setup for femtosecond laser irradiation of PCL (**a**); close up of the processed array–laser scanning direction along x-axis (**b**)

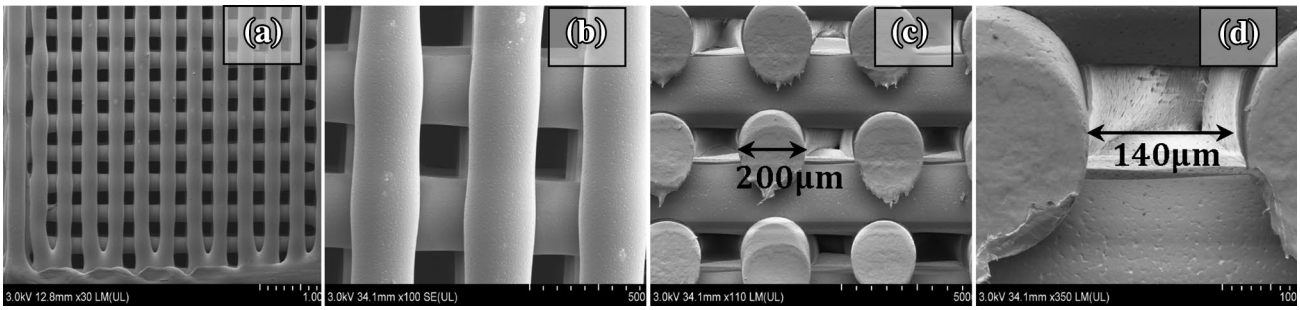

Fig. 3 SEM micrographs of printed PCL fiber meshes: **a, b** front view, **c, d** cross-sectional view

laser treatment at a high-resolution pixel size of 4.4 µm. The X-ray tomograph was operated at a power of 40 kV and a source current of 250 µA. A scanning time of 46.5 min was needed for each sample, with the number of projections being 720. An anisotropic voxel size of 4 µm was achieved in the reconstructed slices.

2.4 Wettability measurements

The contact angle measurements were performed by an OCA contact angle system employing the sessile drop method. Drops of distilled water of 1 µl were gently placed on the surface of processed and non-processed PCL samples using a micro-syringe to measure the angle formed at the liquid–solid interface. Ten measurements were averaged for each sample. The images were captured via a high-speed camera interface.

2.5 Cultivation and viability of MCT3T3 and MG63 osteoblasts cells

The PCL samples were incubated at 37 °C in the presence of 5% CO_2 for 12 h. The non-modified and laser-modified substrates were sterilized by UV light (30 min on both sides). The samples were placed in 48-well suspension culture plates (Greiner Bio-one) and seeded with 100 000 MC3T3 cells in a 0.5-ml culture medium consisting of DMEM (Life Technologies) + 10% fetal bovine serum (Life Technologies). Live/dead analysis was performed 1 and 3 days post-seeding. Live/dead staining [calcein-AM (Anaspec, USA)/propidium iodide (Sigma)] was performed as follows: After rinsing by PBS, the supernatant was replaced by 1 ml of PBS solution supplemented with 2 µl (1 mg/ml) of calcein AM and 2 µl (1 mg/ml) of propidium iodide. The cultures were incubated for 10 min at room temperature, washed twice by PBS solution and evaluated by fluorescence microscopy (Type U-RFL-T, Olympus, Aartselaar, Belgium).

For SEM observation, the samples were fixed following a procedure whereby the specimens were placed in 2% glutaraldehyde (GDA) with a supplement of 2% formaldehyde (PFA) in SCB for 30 min. The samples were then dehydrated by washing in a graded series of 30, 50, 70, 90, and 100% ETOH and finally rinsed in dry alcohol.

3 Results

The femtosecond laser modification performed led to enhanced surface wettability of the PCL constructs.

3.1 SEM and confocal microscopy characterization of laser patterned samples

Previous studies [30] have demonstrated that the surface modification plays a critical role in defining the cells' orientation and direction of migration and proliferation on the biomaterial.

In the work discussed here, we carried out several types of laser modification (continuous irradiation in the form of linear grooves and single or multiple shot irradiations—pits) of the samples to obtain different topographies on the PCL matrix surface. The fluence and the repetition rate of both lasers and the number of applied pulses were varied in a set of experiments to obtain consistent modification. The laser irradiation conditions used to modify the fiber surface properties are listed in Table 1.

Using the above experimental approach, we selected several regimes of processing to gain an optimal interplay between the laser fluence, the number of applied laser pulses and the repetition rate. We concluded that mainly the variation of the laser fluence and the number of applied pulses had a significant effect on the surface modification of the samples processed.

We thus defined the following processing regimes:

Regime type 1 fluence between 1 and 3 J/cm^2, high repetition rate of 1 kHz.

In this case, the sample was processed by continuously scanning the laser beam over the sample surface in the *x* plane. The high-magnification SEM images in Fig. 4 showed that the laser-modified micro-grooved surfaces fabricated

Table 1 Summary of laser irradiation parameters used for processing of 3D PCL samples

Irradiation conditions	Type 1	Type 2	Type 3	Type4	Type 5
Laser fluence (F, J/cm^2)	1; 2; 3	0.1	2	0.2	0.1; 0.2
Number of pulses (N)	Continuous scanning mode	5, 10, 20, 30, 50	20	20	1, 2, 5, 20
Pulse duration (τ, fs)	30	130	130	130	30
Repetition rate (υ)	1 kHz	50 Hz	25 Hz	1 kHz	1 kHz

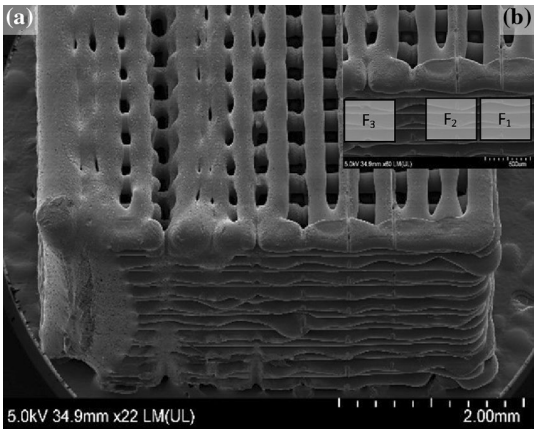

Fig. 4 SEM images of laser-processed grooves on PCL constructs at different laser fluences ($F_1 = 3$ J/cm^2, $F_2 = 2$ J/cm^2, $F_3 = 1$ J/cm^2), $\lambda = 800$ nm, $\nu = 1$ kHz

using multiple laser pulse irradiation had relatively uniform surface morphologies without shape distortion in the low-fluence range. Furthermore, the topography started to change when the fluence was increased above 3 J/cm^2. Signs of melting were visible for higher laser-fluence values (Fig. 4a). Thus, the shape and porosity of the construct were altered, which were most clearly seen in the X-ray computed tomography images.

Regime type 2, 3, 4 (see Table 1)—repetition rate between 25 Hz and 1 kHz and $N = 5$–50.

We further created pit-like structures by patterning with a pre-selected number of laser pulses and varying the laser repetition rate, thus observing the dependence of the crater depth on these parameters. The number of applied laser shots N is determined by Eq. (1).

$$N = \frac{\upsilon \times D}{V}, \tag{1}$$

where ν is the pulse repetition rate, D is the spot diameter and V is the speed of the translation stage motion. The number of laser pulses was varied from 5 to 50, while keeping the speed of the translation stage constant at 2 mm/s.

To follow the effect of the number of applied laser pulses on the PCL fiber meshes, the surface of the scaffold was irradiated at constant laser fluence (0.1 J/cm^2) and repetition rate ($\nu = 50$ Hz) while N was varied from 5 to 50 (Fig. 5). The diameters of the craters ranged from 90 µm (for $N = 50$) to 70 µm (for $N = 5$).

It can be seen from Fig. 5 that by applying low laser fluence values ($F = 0.1$J/cm^2) at $N = 5$, the dimensions of the created pores tend to remain less variable in depth, while by increasing $N = 20$, 30, 50, micropores depth is seriously is altered. The crater depth increased along with the number of applied laser pulses; however, for the whole set of selected parameters, debris around the microstructured area was not visible. The interaction in this low fluence regime results in clean ablation with formation of smooth crater walls, without the signs of melting and resolidification. This could be attributed to the fact that by increasing the number of pulses, the ablated PCL material is fragmented by the oncoming pulses, thus leaving less melt ejection. The process develops with plasma generation and bond scission and some fraction of the material is carried away by the ablated particles. This regime of interaction leads to athermal processing with melt-free zones and the absence of heat-affected zone.

To study the influence of repetition rate on the laser modification, the PCL matrix was irradiated at $\nu = 25$ Hz and $\nu = 1$ kHz, while the number of applied laser pulses was kept constant (Fig. 6).

In the first case, the distance between the separate spots was ~ 100 µm, the distance between two adjacent rows was ~ 250 µm and the number of spots per row was 45. In the second set of irradiation conditions, the distance between the separate spots was ~ 80 µm, the distance between two adjacent rows was ~ 150 µm and number of spots per row was 60. The sample translation speed for both cases was kept at 2 mm/s.

The processed zone is affected by the heat accumulation effect. From Fig. 6, it is visible that at low values of repetition frequencies and high laser fluence values, no side effects could be observed in crater surrounding. Generation of melt ejection at circumferential areas of the irradiated zones, leading to a higher degree of surface roughness, is observed at increased repetition frequencies and low laser fluence values. In the case of high repetition frequency, the time between two consecutive pulses is very small and, thus, the time for heat diffusion is very limited, leading to energy accumulation and temperature increase in the processed zone. This localized heating forms melt ejection.

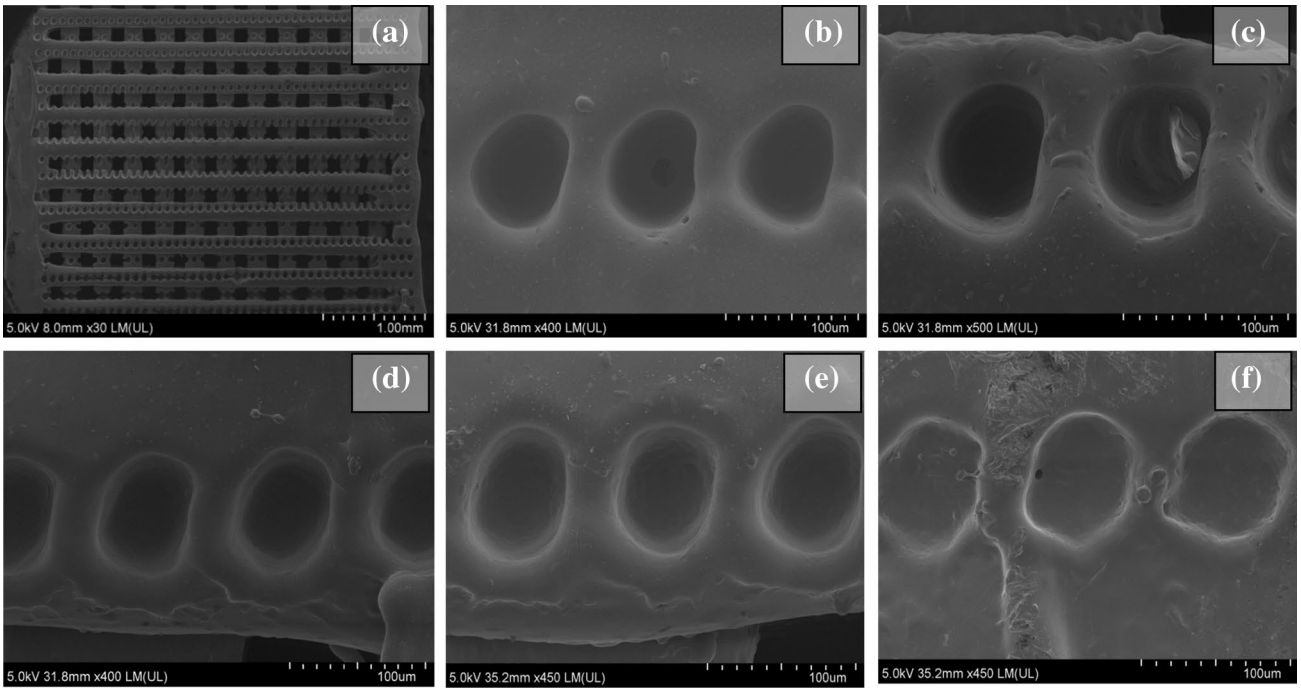

Fig. 5 SEM images of laser ablated craters on PCL fiber meshes when varying N at constant laser fluence ($F = 0.1$ J/cm^2), repetition rate ($\nu = 50$ Hz) and $\tau = 130$ fs; **a** overall front view; **b** $N = 50$; **c** $N = 30$; **d** $N = 20$; **e** $N = 10$; **f** $N = 5$

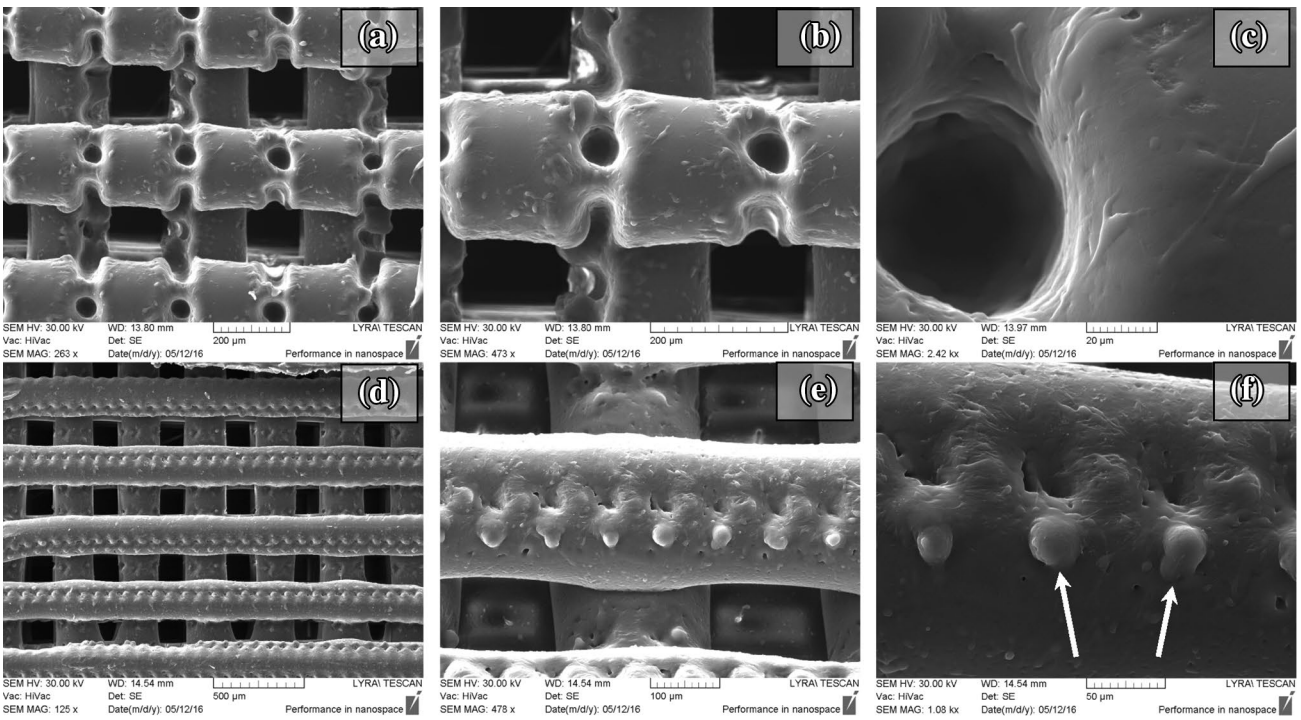

Fig. 6 SEM images of PCL constructs after femtosecond laser processing at **a–c** $F = 2$ J/cm^2, $\nu = 25$ Hz, $\tau = 130$ fs, $N = 20$; **d–f** $F = 0.2$ J/cm^2, $\nu = 1$ kHz, $\tau = 130$ fs, $N = 20$

To circumvent this consequence, by reducing the repetition rate and increasing the laser fluence, this side effect could overcome.

Regime type 5 low laser fluence between 0.1 and 0.2 J/cm^2, high repetition rate of 1 kHz.

Figure 6d–f shows a side effect of the irradiation at a repetition rate of 1 kHz, namely the formation of bump-like structures in the vicinity of the craters (white arrows).

The modification of the PCL scaffold at a 1-kHz repetition rate was further analyzed by confocal microscopy. Figure 7 shows the topography, reconstructed 3D images and cross-sections of the reconstructed images of 160 µm × 160 µm areas of PCL fibers modified by irradiation by 1, 2 and 5 pulses, at $F = 0.1$ J/cm^2, $\tau = 30$ fs, 1 kHz. In the cases of one and two pulses, a protrusion is formed, which grows in height to approximately 8–10 µm above the base level (Fig. 7a, b). When the number of applied laser pulses is raised to five, the protrusion collapses and a concavity is formed in the middle of the modified zone with signs of molten re-solidified material around the center of the interaction zone (Fig. 7).

In this specific case of fs laser processing with reduced pulse width duration to $\tau = 30$ fs and high repetition rate (1KHz), the laser fluence remains lower than the ablation threshold value, but high enough to realize other effects such as surface material expansion followed by startup of crater formation when number of applied laser pulses (N) is > 5. The rapid energy deposition on a fiber surface forms shock waves and develops high pressure gradient in the interaction zone. This pressure development initiates the formation of cavitation bubbles on the polymer rod (Fig. 7a, b).

Similar effects were observed as the laser fluence was increased further (Fig. 8a). Irradiation by a single pulse produced again a bump-like structure. After drastically increasing the number of applied laser pulses to 20, we noted the creation of craters with a depth as shown in the

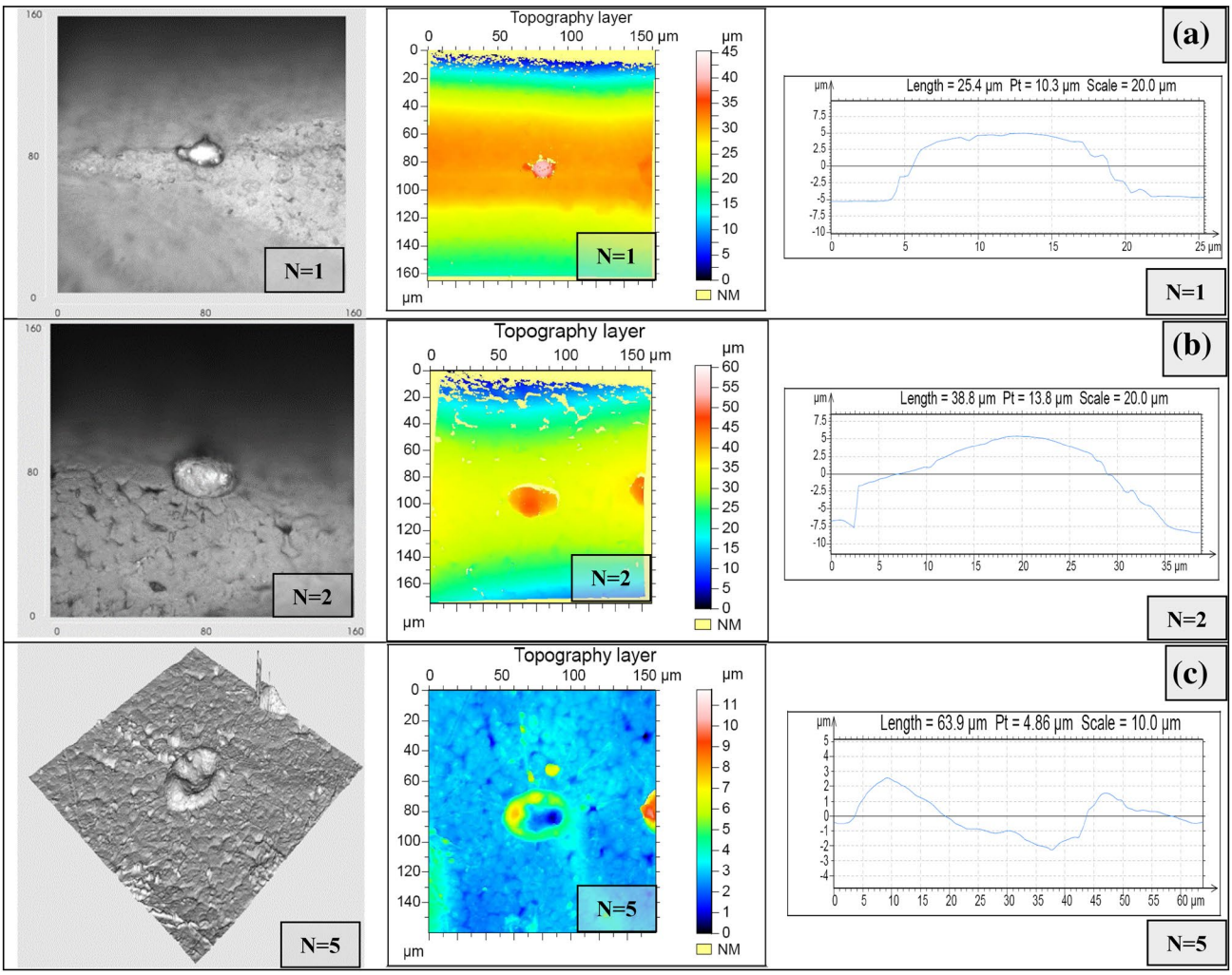

Fig. 7 Confocal microscopy image of the laser-induced modification formed at $F = 0.1$ J/cm^2, $\tau = 30$ fs, $\nu = 1$ KHz repetition rate, focal length lens 20 cm; **a** topography, 3D reconstructed image and cross-section of the 3-D reconstructed image at $N = 1$; **b** at $N = 2$; **c** at $N = 5$

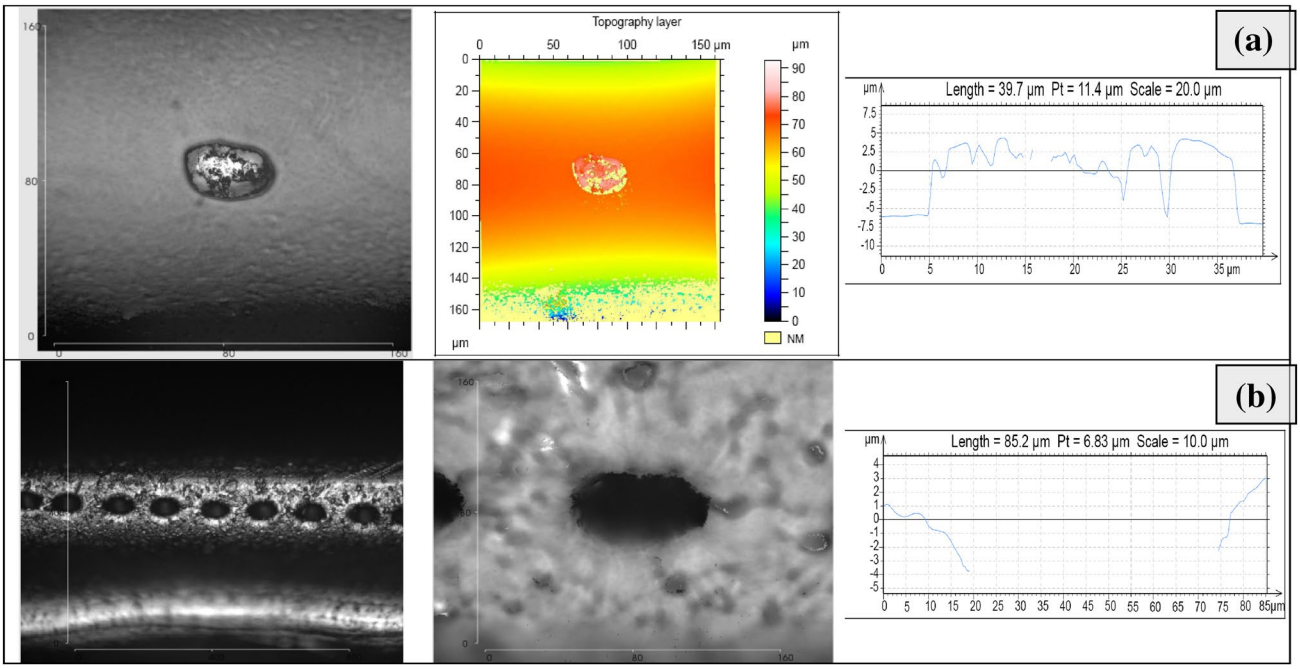

Fig. 8 Confocal microscope image of the laser-induced modification at $F = 0.2$ J/cm^2, $\tau = 30$ fs, 1 kHz repetition rate, lens focal length 20 cm; **a** topography, 3D reconstructed image and cross-section of the reconstructed 3D image at $N = 1$; **b** topography and cross-section of the reconstructed 3D image at $N = 20$

cross-section reconstruction of the confocal microscopy image in (Fig. 8b).

The laser processing induced additional topography features on the PCL scaffold surface, namely formation of craters at the surface of a single fiber. The laser ablation of polymers in regime type 5, proceeds with minimized heat diffusion into the sample due to the extremely short pulse widths and removal of the material is initiated with high precision without thermal damage of the surroundings areas. Malinauskas et al. [31] reported that the micro-/nano-structuring could influence the surface roughness which affects the cellular morphology and proliferation. They manufactured microporous structures (holes and shaped the outer geometries) of polylactic acid (PLA) with fully controllable porosity by employing direct laser writing (DLW).

3.2 Quantitative analysis of the PCL scaffold

3D models of the scaffolds were generated based on the µCT scans. The porosity of the scaffolds was determined using a CT Analyzer (Bruker). The high-resolution tomography images provide information about the morphology of the scaffold by measuring the porosity of the structure, the fibers' diameter and the distance between the fibers Table 2.

In a further experiment, we performed surface patterning by continuous scanning of the laser beam at various laser fluences over the fiber surface to form grooves; we observed

Table 2 Parameters of PCL scaffolds before and after laser irradiation as determined by X-ray computed tomography (mean value ± standard deviation)

Parameters	Before laser treatment	After laser treatment
Porosity (%)	40.4 ± 0.3	38 ± 0.5
Average fibre diameter (µm)	209.9 ± 0.5	210.9 ± 0.5
Average distance between the fibres (µm)	147.9 ± 4.8	154.5 ± 18.1

severe alteration of the scaffold shape in the high-fluence range, thus reducing the porosity Table 2 of the matrix. Value of the porosity decreased about 2% after laser treatment. Based on binarization of 8-bit images, an error of the method was calculated. Threshold of binarization was designated as a minimum value between air and scaffold peak. Variation of that value with ± 1 allowed to reckon an error of the method resulting with 0.4%.

Figure 9a shows reconstructed 3D images of the sample revealing its architecture before laser treatment. Figure 9b demonstrates the alternation of the fibers form from one layer to the adjacent layer after laser irradiation.

Figure 9b presents the laser-induced defects and melting between adjacent layers at a laser fluence of 3 J/cm^2. The tomography images obtained provide an insight of the

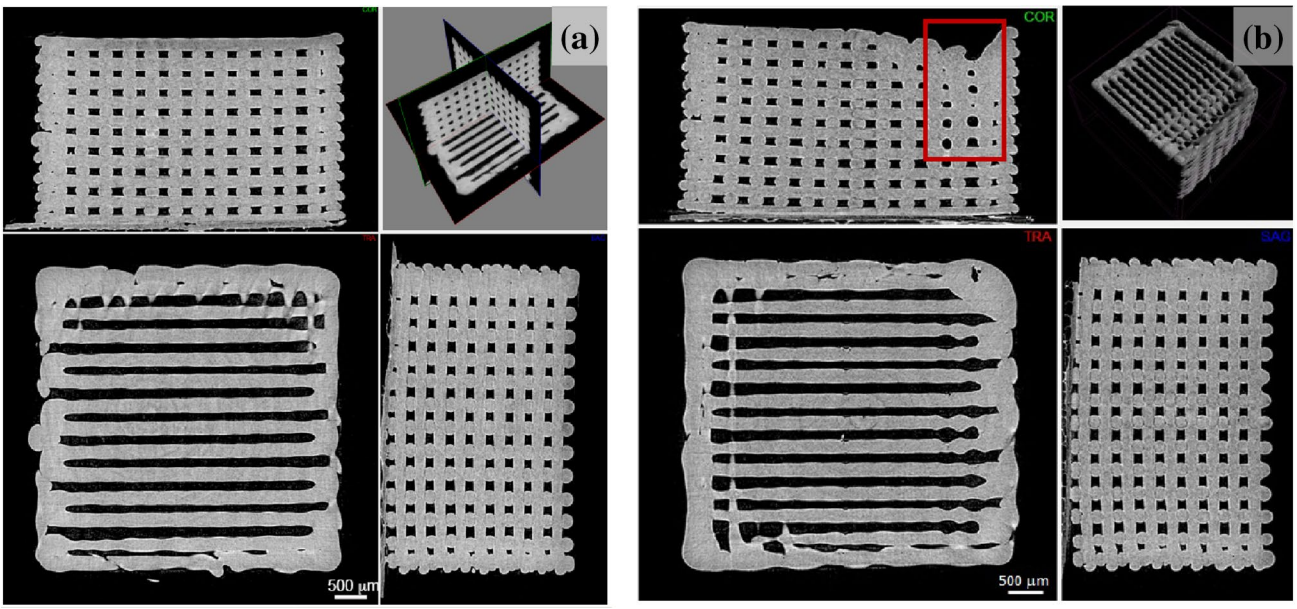

Fig. 9 X-ray tomography images of three cross-sections of a PCL polymer scaffold and its spatial representation: **a** before laser treatment, **b** after laser treatment—linear grooves patterning, $F = 1$, 2 and 3 J/cm^2, repetition rate 1 kHz, $\tau = 30$ fs

scaffold structure and the material behavior in depth after laser treatment. It permits one to define the best irradiation condition in view of obtaining precise structuring of the specimen. The laser fluence must be kept below 3 J/cm^2 to avoid the initiation of melting (in the case of continuous irradiation conditions).

3.3 Wettability change: varying laser power, number of laser pulses

We compare below the results of the water contact angle measurements for non-irradiated and laser irradiated PCL samples. The surface wettability measurements before and after laser femtosecond treatment revealed a change in the contact angle value of the PCL surface from $85° \pm 2°$ to $59° \pm 2°$ at time zero, indicating that this treatment induced changes in the surface properties of the PCL meshes (Fig. 10). The water contact angle of a non-laser-irradiated PCL matrix was taken as a reference (Fig. 10a).

The water contact angle was minimal, 59°, when the sample surface was treated by 40 laser pulses; i.e., increasing the number of laser pulses applied at a constant laser fluence affected the material's surface roughness by increasing its hydrophilicity.

3.4 Surface modification effect on the osteoblasts cells growth

The extracellular matrix (ECM) is a micro-environment where cells adhere, proliferate and migrate. Substituting this complex structure by an artificial scaffold would require that the latter should possess many essential features, one

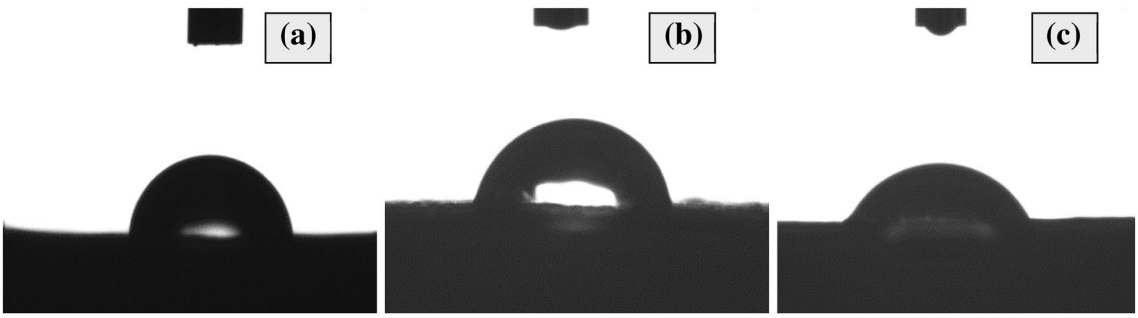

Fig. 10 Images of contact angles of microscopic distilled water droplets on **a** flat, $\theta_w = 85° \pm 2°$ and **b, c** patterned ($N = 20$ and 40, $\tau = 130$ fs, $F = 0.1$ J/cm^2), $\theta_w = 81° \pm 2°$, $59° \pm 2°$, PCL surfaces

among them being the porosity, as it plays a critical role in diverse cellular processes [32, 33]. We prepared a series of micropatterned PCL surfaces with various sizes and cultured MC3T3 (osteoblast), MG63 (osteoblast) cells on the modified surfaces. The results indicated excellent localization of the cells on the patterned PCL matrices.

Live/dead images were obtained of the substrates/scaffolds seeded with MC3T3 cells and cultured for one and three days (Fig. 11). The viability of the osteoblastic cells that are seeded onto the PCL scaffolds is evaluated with a live/dead staining. Live cells are stained with calcein-AM and dead cells are stained with propidium iodide resulting in fluorescent photographs of green (live) and red (dead) cells as presented in (Fig. 11).

This analysis showed the excellent biocompatibility of the scaffolds. The spread cell morphology indicated that the cells adhered well to the non-modified and the laser-modified samples. Cell attachment on non-modified scaffolds was only visible on the first polymer strut. This observation contrasted with the case of laser-modified PCL scaffolds, where attached cells could be observed on the underlying PCL struts. During the following days, the cells continued to grow, the structures being almost entirely covered with viable cells. The MCT3T3 cell cultivation tests (Fig. 11) demonstrated that the laser-processed PCL samples allowed good cell proliferation in volume compared to the non-processed samples. Native PCL is a hydrophobic polymer where cell attachment is limited. In the present article, increased adherence is the result of surface roughness and change in hydrophobicity demonstrated via either SEM or contact angle measurement. The chemical modification of the PCL will be analyzed in future studies, but it has been shown in literature that a change in surface hydrophilicity can be the result of chemical modification Ghobeira et al. [34].

3.5 Evaluation of MG63 osteoblasts cells growth using SEM

In this study, we addressed the biological performance of the laser-textured PCL fiber meshes in an attempt to find if the introduction of additional roughness and porosity by the created micro-craters would affect the cells' viability and infiltration.

Disadvantages of PCL is its hydrophobicity and lack of functional groups, resulting in poor cell attachment and proliferation. To enhance cell attachment and colonization,

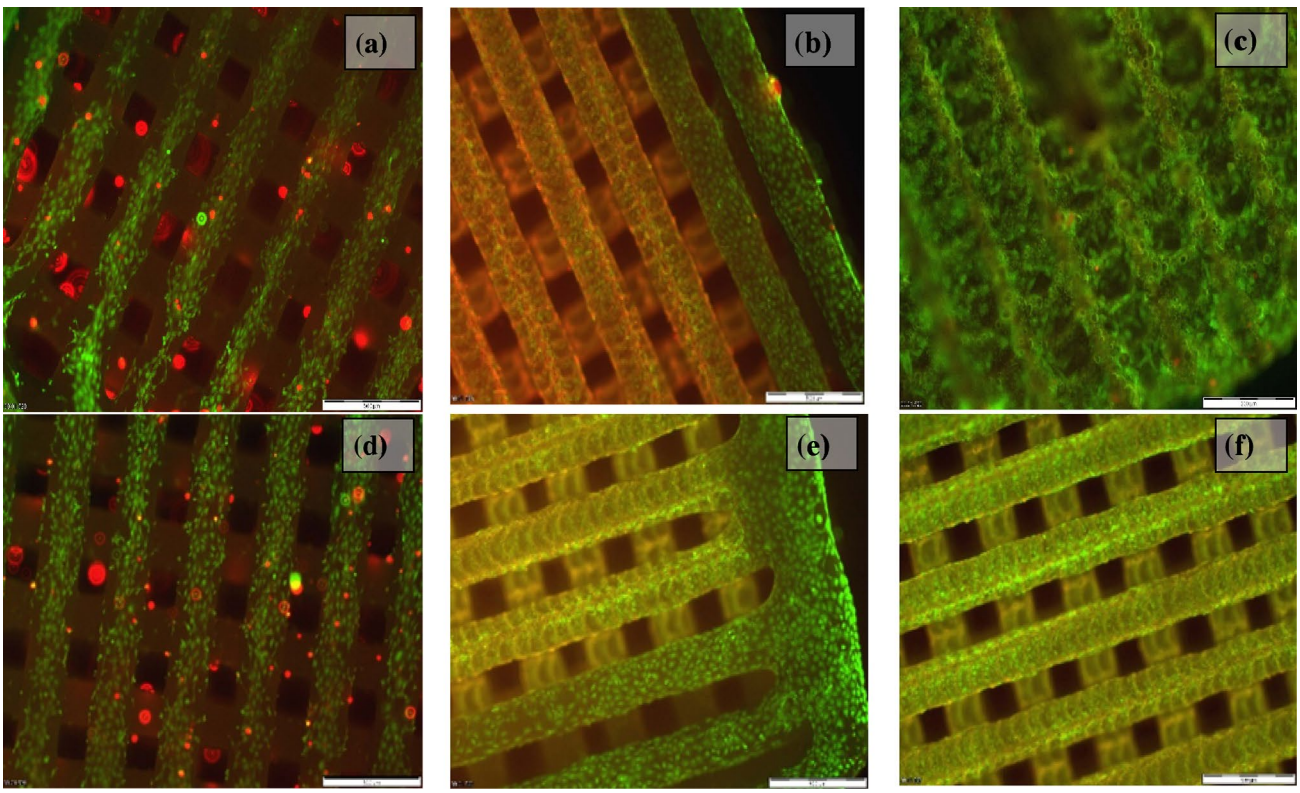

Fig. 11 MC3T3 osteoblasts cell adhesion and proliferation on PCL scaffolds: **a** cell adhesion on control (non-modified) PCL scaffolds, **b, c** cell adhesion into laser created craters ($N=5$, $\nu=50$ Hz, $F=0.1$ J/cm^2) after 1-day culturing; **d** cell proliferation on control (non-modified) PCL scaffolds, **e, f** MC3T3 proliferation into laser created craters ($N=5$, $\nu=50$ Hz, $F=0.1$ J/cm^2) after 3-day culturing. Fluorescence microscopy after live/dead staining. Scale bar **a, b, d, e** 500 µm; scale bar **c, f** 200 µm

several surface modifications techniques of PCL have been developed, including laser surface modification Tiaw et al. [35], ion beam radiation Pignataro et al, [36], plasma modification Yildirim et al. [37], Ghobeira et al. [38], chemical modification Cheng et al. [39] and combinations thereof Declercq et al. [40]. As described by Ghobeira et al. [34] and Lasgorceix et al. [41] surface modification is the result of a synergistic effect of surface roughness, changes in hydrophibicity and chemical modification. The acquired results from wettability measurements (Fig. 10) showed that with increasing pulse number (*N*) at constant laser fluence, surface hydrophilicity is improved. This improvement could be attributed to difference in chemical structure of the modified regions. Another option is that laser patterning develops oxide formation at the treated zones and interact with the broken PCL chemical bonds via photodecomposition mechanisms Tiaw et al [35].

The laser-induced additional porosity of the PCL matrix has been used to enhance the contact guidance phenomenon, a mechanism responsible for cell locomotion. It is dependent on biochemical, morphological and topographical stimuli [42]. The surface roughness affects the cells' receptivity due to changes in the extracellular matrix protein adsorption on modified zones. These findings demonstrate that cells can be confined to precise locations, through the creation of laser-ablated craters on fiber meshes without inducing side effects on cell viability.

By laser-assisted technique, spatial control of cellular movement could be achieved by preserving scaffold integrity.

The effect of laser-induced microporosity on MG63 osteoblasts outgrowth was evaluated using SEM microscopy (Fig. 12). The MG63 osteoblast cells were cultured for 7 days. Before the cell-seeding procedure, the samples were exposed to UV irradiation for 30 min (on each side) and rinsed with PBS to remove any contamination.

The MG63 cells showed a directional orientation toward the laser-created craters, providing a network for ingrowth in the depth of the concavities formed. We should note the topography guidance of the MG63 cells. Thus, we registered a modified response of the cells to the surfaces whose properties were modified by laser treatment, namely, it is evident that the induction of additional porosity facilitated cell infiltration.

4 Discussion

Numerous studies on laser treatment of diverse kinds of polymers have been reported and various ablation models have been proposed involving selection of many ablation and material parameters [43–45]. The laser ablation mechanism classification strongly depends on the type of polymer used on the one hand, and on the type of laser source used for processing, on the other. There is a distinct difference between the ablation mechanisms in the nanosecond and femtosecond time domains. Among the widely studied polymers are polymethylmethacrylate (PMMA), polyimide, polyethylene terephthalate (PET), Teflon™.

Diverse controversial discussions concerning the mechanism of nanosecond laser ablation (photochemical, thermal/photothermal models) had been taken place during the years. However, it comes to a general agreement that in ns pulses the energy of the photons is transformed into the energy of electronic excitation [46]. For example, for polymers, it is generally believed that the pure photochemical ablation mechanism takes place due to direct bond breaking when UV photons are applied. However, Morshedian et al. [47]

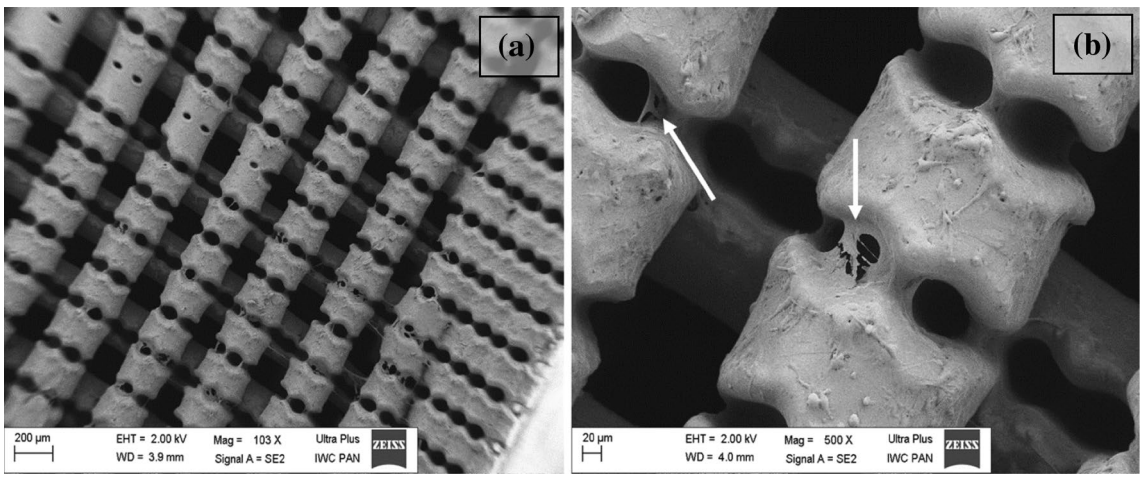

Fig. 12 SEM microscopy images of the surface roughness effect on MG63 cells proliferation after 7 days of cultivation, scale bar **a** 200 µm; **b** 20 µm

reported that, at energies of 110–140 mJ and a 1064 nm wavelength and pulse duration of 20 ns, both processes, chemical changes (due to heating) and photochemical effect are involved in the ablation of polymethylmethacrylate (PMMA) polymer samples.

Ultrafast laser ablation develops when the applied laser energy density exceeds a certain threshold related to the molecular binding and ionization energies of the material.

The primary mechanism suggested for femtosecond-laser-pulse interaction with polymers is multiphoton absorption [48]. The absorption mechanisms could deviate according to the type of absorbing materials [metals, semiconductors, transparent dielectric materials (glasses and polymers)]. Thus, the absorption process can be linear for metals or a nonlinear for transparent materials. In the case of the linear absorption, the heated electrons, due to photon absorption, transfer the thermal energy to the lattice, triggering melting or vaporization of the material. The nonlinear process—multiphoton absorption—is dominant in the case of dielectrics and transparent materials. The ablation process is initiated via energy absorption by bound and free electrons, triggering excitation and ionization, by simultaneously absorbing a number of *n* photons. The number of absorbed photon times' photon energy has to be larger than the ionization potential or bandgap. The following energy transfer to the atomic subsystem leads to bond breaking and material expansion [49].

For example, if the wavelength of a laser is 800 nm, the photon energy is calculated to be 1.55 eV, thus it is required at least 4 photon absorption for a material with 6 eV ionization potential (most of the polymers have ionization potential ranging from 4 to 7 eV) [50]. The ablation develops without formation of heat-affected areas due to the short interaction time of the order of picoseconds.

Most of the previous reports [51] have dealt with femtosecond laser processing of electrospun fiber meshes; single case studies on laser post-modification of 3D printed PCL scaffolds have only been published [52].

By varying the laser parameters, one can generate morphological modification of the surface of a polymer scaffold. The number of laser pulses applied (influencing the craters' depth) and the laser pulse repetition rate and fluence (affecting the craters' modifications) have been found to impact significantly the PCL surface morphology. Most of the observations were related to the lack of swelling in the zones of interaction. The effects on the crater formation notwithstanding the overall basic woodpile structure have been found to remain intact; only in the case of grooves (patterning in the higher energy range) distortion of the 3D structure has been seen due to the melting of the polymer material.

We monitored the pulse duration dependence for two pulse-duration values, 30 and 130 fs; no significant differences were detected. In the fs interaction regime, the heat diffusion into the processed material is minimal, leading to optimal processing of the material with negligible heat-affected zones. The fast energy absorption leads to bond breaking and expansion of the material. Thermal side effects, in this case, are negligible since melting takes place on a time scale of less than 1 ps, leading to clean ablation without formation of heat-affected zones [53]. This results in a precise structuring of the PCL cubes with extremely small heat diffusion and negligible side effects to the surrounding zones and makes it possible to circumvent the undesired additional fibers modification.

Besides the specific properties that characterize the femtosecond laser–matter interaction, other factors that one should consider are the thermal properties of the polymer, namely specific heat capacity, absorption coefficient, diffusivity, and density.

The thermal conduction length corresponding to the femtosecond laser pulse duration is small; thus, the absorbed energy diffusion is limited [54]. Ionization and ablation processes start to develop when the laser fluence exceeds a threshold that is specific for each material. In the experiments employing a certain number of laser pulses, the measured crater diameters have been found to deviate by 10–30 μm from the focused laser-light spot dimension. This observation could be attributed to the formation of plasma during the process of interaction. The formation of a plasma plume in air has been detected during processing; thus, the difference in the craters' dimensions could be explained by the plasma expansion; materials such as PCL with low thermal conductivity (0.07 W/m K) and heat capacity (1.3 kJ/kg K) are assumed to be susceptible to this effect.

We made another important observation in the low-fluence regime at a 1-kHz repetition rate, a pulse duration of 30 fs, and a low number of applied laser pulses (≤ 2); this regime of interaction creates bubble-like structures formed due to increased pressure in the zone of interaction leading to expansion of the material. The rapid energy delivery in a thin surface layer leads to an extremely high energy density, formation of intense shock waves and a large pressure gradient in the interaction zone. When the number of applied laser pulses is increased to five at a fixed fluence, the bubble structure loses its uniformity, an intermediate liquid–gas state is generated followed by nucleation; the material is overheated above melting point until a critical bubble forms which finally explodes with melted filaments remaining near the crater.

In the case of linear grooves patterning, the higher energy input is converted to thermal energy and triggers melting and evaporation of the PCL material, which has a relatively low melting point (57 °C).

By performing cell culturing experiments, we tested the effect of laser processing on the fiber meshes. The results proved that the laser irradiation treatment does not bring about additional side effects, so that the functionality of the

scaffolds is preserved. The surface morphology produced was shown to provide a directional orientation of both types of osteoblasts cells, which in turn would shorten the tissue formation time. The possibility to control the cellular dynamics within a 3D structure by inducing additional porosity using a laser-based method could contribute to the future development of novel implant designs.

5 Conclusion

In this study, we proposed a combination of a femtosecond-laser modification method and a 3D FDM printing technique to achieve efficient production and post-processing of biomimetic and biodegradable poly-ε-caprolactone (PCL) scaffolds. Our primary aim was to induce an additional laser-based modification of polymer PCL scaffolds with microfeatures, which would contribute to increasing the porosity of the matrix, thus enhancing the cell ingrowths in volume. The 3D woodpile scaffolds were fabricated by a 3D printing method; laser post-modification was applied to woodpile constructs creating craters on the surface of the fibers. We demonstrated the possibility to create different types of patterns (grooves and pits), following the effects of varying the laser parameters and found that the laser pulse repetition rate, fluence, and number of applied pulses influence drastically the form of the modifications produced. Using high-resolution X-ray tomography images, we also characterized the laser irradiation influence on the sample in its volume.

Our results from studying cell cultivation on modified PCL constructs demonstrated an enhanced viability of different cell cultures, namely MG63 osteoblasts and MCT3T3 cells, in the laser-created patterns. The research performed showed that the femtosecond laser is a promising contactless tool that can be successfully employed to improve the hydrophilic properties of the PCL material.

Acknowledgements This work was financially supported by the Bulgarian National Science Fund under project No. DN08/5/2016-2018; by DNTS Austria 01/1/2013-2017; by COST MP1301 NEWGEN; by project FWO/BAS "Functionalization of biomaterials modified by femtosecond pulses for cell adhesion and guidance improvement" (2016–2019); and by NewJoint.

References

1. C. Bashur, L. Dahlgren, A. Goldstein, Biomaterials **27**, 5681 (2006)
2. M. J. Chern, L. Yang, Y. Shen, J. Hung, Int. J. Precis. Eng. Manuf. **14**, 2201 (2013)
3. H. Yu, P. Wooley, S.Yang, J. Orthop. Surg. Res. **4**, 1–9 (2009)
4. F. Hajiali, S. Tajbakhsh, A. Shojaei, Journal Polymer Reviews **1** (2017)
5. Y. Ding, W. Li, T. Müller, D. Schubert, A. Boccaccini, Q. Yao, J. Roether, ACS Appl. Mater Interfaces **27**, 17098 (2016)
6. S. Sharma, D. Gupta, S. Mohanty, M. Jassal, A. Agrawal, R. Tandon, Invest. Ophthalmol. Vis. Sci. **55**(2), 899 (2014)
7. Y. Hosseini, R. Emadi, M. Kharaziha, A. Doostmohammadi, J. Appl. Polym. Sci. **134**, 44433 (2017)
8. C. Grandi, R. Di Liddo, P. Paganin, S. Lora, D. Dalzoppo, G. Feltrin, C. Giraudo, M. Tommasini, M. Conconi, P. Parnigotto, Int. J. Mol. Med. **27**, 455 (2011)
9. H. Yu, H. Matthew, P. Wooley, S. Yang, J. Biomed. Mater. Res. Part B Appl. Biomater. **86B**, 303 (2008)
10. M. Alves, I. Pashkuleva, R. Reis, J. Mano, Small **10**, 1 (2010)
11. Y. Chung, Y. Chiu, J. Med. Biol. Eng. **29**, 320 (2009)
12. X. Liu, P. Chu, C. Ding, Mater. Sci. Eng. R **70**, 275 (2010)
13. D. Falconnet, G. Csucs, H. Michelle, J. Grandina, M. Textor, Biomaterials **27**, 3044 (2006)
14. K. Moraczewski, P. Rytlewski, R. Malinowski, M. Zenkiewicz, Appl. Surf. Sci. **346**, 11 (2015)
15. A. Manakhov, E. Kedroňová, J. Medalová, P. Černochová, A. Obrusník, M. Michlíček, D. Shtansky, L. Zajíčková, Mater. Des. **132**, 257 (2017)
16. K. Sugioka, Y. Cheng, Light Sci. Appl. **3**, 1 (2014)
17. K. Deepak, V. Soma, N. Desai, *Direct Writing in Polymers with Femtosecond Laser Pulses: Physics and Applications* (InTech, 2012), p. 277. https://doi.org/10.5772/45854
18. G. Turnbull, J. Clarke, F. Picard, P. Riches, L. Jia, F. Han, B. Li, W. Shu, Bioact. Mater. (2017). https://doi.org/10.1016/j.bioactmat.2017.10.001
19. J. Zeltinger, J. Sherwood, D. Graham, R. Müeller, L. Griffith, Tissue Eng. **7**, 557 (2001)
20. Y. Lim, J. Johnson, Z. Fei, Y. Wu, D. Farson, J. Lannutti, H. Choi, L. Lee, Biotechnol. Bioeng. **108**, 116 (2011)
21. C. Simitzi, P. Efstathopoulos., A. Kourgiantaki, A. Ranella, I. Charalampopoulos, C. Fotakis, I. Athanassakis, E. Stratakis, A. Gravanis, Biomaterials **67**, 115 (2015)
22. V. Dinca, L. Sima, L. Rusen, A. Bonciu, T. Lippert, M. Dinescu, M. Farsari, *Bio-Interfaces Engineering Using Laser-Based Methods for Controlled Regulation of Mesenchymal Stem Cell Response In Vitro* (InTech, 2016), p. 221. https://doi.org/10.5772/61516
23. C. Yan, J. Sun, J. Ding, Biomaterials **32**, 3931 (2011)
24. M. Cutiongco, S. Goh, R. Launais, C. Visage, H. Low, E. Yim, Biomaterials **84**, 184 (2016)
25. A. Riveiroa, R. Sotoa, R. Comesana, M. Boutinguizaa, J. del Vala, F. Quinteroa, F. Lusqui˜nosa, J. Pou, Appl. Surf. Sci. **258**, 9437 (2012)
26. Z. Ma, Z. Mao, C. Gao, Colloids Surf. B **60**, 137 (2007)
27. S. Mishra, V. Yadava, Opt. Lasers Eng. **73**, 89 (2015)
28. J. Reif, in *Laser-Surface Interactions for New Materials Production*, ed. by A. Miotello, P. Ossi. Basic Physics of Femtosecond Laser Ablation, Springer Series in Materials Science, vol. 130 (Springer, Berlin, Heidelberg, 2010)
29. M. Liu, Opt. Lett. **7**, 196 (1982)
30. A. Matsugaki, G. Aramoto, T. Ninomiya, H. Sawada, S. Hata, T. Nakano, Biomaterials **37**, 134 (2015)
31. M. Malinauskas, S. Rekštyt, L. Lukoševicius, S. Butkus, E. Balciunas, M. Peciukaityt, D. Baltriukien, V. Bukelskien, A. Butkevicius, P. Kucevicius, V. Rutkunas, S. Juodkazis, Micromachines **5**, 839 (2014)
32. P. Danilevicius, L. Georgiadi, C. Pateman, F. Claeyssens, M. Chatzinikolaidou, M. Farsari, Appl. Surf. Sci. **336**, 2 (2015)
33. E. Fadeeva, A. Deiwick, B. Chichkov, S. Schlie-Wolter, Interface Focus **4**, 1 (2016)
34. R. Ghobeira, C. Philips, H. Declercq, P. Cools, N. Geyter, R. Cornelissen, R. Morent, Biomed. Mater. **12**, 015017 (2017)
35. K. Tiaw, S. Goh, S.M. Hong, Z. Wang, B. Lan, S. Teoh, Biomaterials **26**, 763 (2005)

36. B. Pignataro, E. Conte, A. Scandurra, G. Marletta, Biomaterials **18**, 1461 (1997)
37. E.D. Yildirim, S. Güçeri, W. Sun, Plasma Process. Polym. **8**, 256 (2011)
38. R. Ghobeira, C. Philips, V. Naeyer, H. Declercq, P. Cools, N. Geyter, R. Cornelissen, R. Morent, J. Biomed. Nanotechnol. **13**, 699 (2017)
39. Z. Cheng, S. Teoh, Biomaterials **25**, 1991 (2004)
40. H. Declercq, T. Desmet, E. Berneel, P. Dubruel, M. Cornelissen, Acta Biomater. **9**, 7699 (2013)
41. M. Lasgorceix, C. Otta, L. Boilet, S. Hocquet, A. Leriche, M. Asadian, N. Geyter, H. Declercq, V. Lardot, F. Cambier, Mater. Sci. Eng. C. (2018). https://doi.org/10.1016/j.msec.2018.03.004
42. S. Cio, J. Gautrot, Acta Biomater. **30**, 26 (2016)
43. M. Brown, C. Arnold, *Fundamentals of laser-material Interaction and application to multiscale surface Modification* (Springer, Berlin, 2010)
44. S. Baudach, J. Bonse, W. Kautek, Appl. Phys. A **69**, 395 (1999)
45. M. Hashida, H. Mishima, S. Tokita, S. Sakabe, Opt. Express **17**, 13116 (2009)
46. T. Lippert, Adv. Polym. Sci. **168**, 51 (2004)
47. N. Morshedian, Plasma Sci. Technol **19**, 095501 (2017)
48. M. Zamfirescu, M. Ulmeanu, A. Bunea, G. Sajin, R. Dabu, in *Recent Advances in Nanofabrication Techniques and Applications*, ed. by B. Cui. Ultrashort pulsed lasers—efficient tools for materials micro-processing (InTech, 2011). ISBN: 978-953-307-602-7
49. F. Korte, J. Serbin, J. Koch, A. Egbert, C. Fallnich. A. Ostendorf, B. Chichkov, Appl. Phys. A **77**, 229 (2003)
50. K. Deepak, S. Venugopal Rao, D. Narayana Rao, Proc. of SPIE **8190**, 81900R-1 (2011)
51. B. Lee, H. Jeon, A. Wang, Z. Yan, J. Yu, C. Grigoropoulo, S. Li, Acta Biomater. **8**, 2648 (2012)
52. L. Jonusauskas, E. Skliutas, S. Butkus, M. Malinauskas, Lith. J. Phys. **55**, 227 (2015)
53. C. Aguilar, Y. Lu, S. Mao, S. Chen, Biomaterials **26**, 7642 (2005)
54. H. Choi, D. Farson, J. Lannutti, J. Laser Appl. **19**, 225 (2007)